Catalysis Today 157 (2010) 446–450

Contents lists available at ScienceDirect

Catalysis Today

journal homepage: www.elsevier.com/locate/cattod

Doped $LaFeO_3$ as SOFC catalysts: Control of oxygen mobility and oxidation activity

Nandita Lakshminarayanan[a], John N. Kuhn[a], Sergey A. Rykov[b], Jean-Marc M. Millet[c], Umit S. Ozkan[a,*]

[a] The Ohio State University, Department of Chemical and Biomolecular Engineering, Columbus, OH 43210, USA
[b] Department of Chemical Engineering, University of Delaware, Newark, DE 19716, USA
[c] CNRS-Institut de Recherche sur la Catalyse et l'Environnement de Lyon, Université Claude-Bernard, 69626 Villeurbanne Cedex, France

ARTICLE INFO

Article history:
Available online 27 April 2010

Keywords:
Perovskite
Solid oxide fuel cell
Oxygen nonstoichiometry
Structure–property
Oxidation activity
Chemical compatibility

ABSTRACT

The bulk structure and surface properties of Fe-based perovskite-type oxides with the formula $La_{0.6}Sr_{0.4}Co_yFe_{1-y}O_{3-\delta}$ for $y = 0.1$, 0.2, and 0.3 have been investigated. The properties were found to strongly depend upon Co content, temperature, and environment. The materials were selected due to their potential use as solid oxide fuel cell cathodes. The intermediate Co loading formed oxygen vacancies most easily and several other properties including oxidation activity and surface sites showed a similar non-linear trend. Trends are related to a possible transition in electronic structure. Activity for oxidation of methane, oxygen storage and chemical compatibility was shown to be superior to that of the $La_{0.6}Sr_{0.4}MnO_3$.

1. Introduction

Perovskite-type (ABO_3) oxide catalysts have been studied extensively over the past several years due to their unique oxygen storage and conduction properties [1–3]. Their properties render them useful for several catalytic applications including total and partial oxidation reactions of hydrocarbons and volatile organics, photo catalysis, and environmental applications such as SO_2 removal. They are also widely studied and used in oxygen sensors and oxygen separation membranes where their anionic conductivity is utilized to achieve high purity separations [4,5]. The main focus of the present work is to study the Fe- and Co-based perovskite oxides as potential cathode electrocatalysts for solid oxide fuel cells.

Although Co-based materials were the first perovskite-type oxides studied as SOFC cathodes, Mn-based materials gained popularity because of their increased stability at the high operating temperatures [6]. However the Mn-based materials do not perform well at lower temperatures and limit SOFC performance. Fe- and Co-based oxides, on the other hand, are expected to improve performance due to higher ionic conduction characteristics even at much lower operating temperatures (500–800 °C). These materials have improved oxygen reduction and conduction capabilities due to their defect structure and presence of oxygen vacancies [4]. As the ionic conductivity increases, the electrochemically active reaction area for the oxygen reduction reaction in solid oxide fuel cell cathodes expands beyond the triple phase boundary (the interface between cathode/electrolyte/gas phase oxygen). Research regarding the use of Co-based SOFC cathodes has shown that in these materials, bulk ionic transport and the surface exchange kinetics of the oxygen reduction reaction (ORR) co-limit SOFC performance [7]. Thus in these materials both the bulk-oxygen pathway as well as the interfacial oxygen reduction kinetics play an important role. It has been shown that surface processes that are chemical in nature such as the surface oxygen exchange and oxygen surface diffusion, influence the performance of mixed conducting perovskite-type materials [4,7–11].

Oxygen ion mobility is an important property desired for SOFC performance. In solid oxide materials, oxygen ions are transported by the random hopping of oxygen vacancies in the anion framework of the materials. Oxygen vacancies are formed by charge imbalances induced by doping of the materials. In perovskite-type materials, it generally occurs by doping the normally trivalent A-site (La) with a divalent cation (Sr). Also, the creation of oxygen vacancies is a strong function of environment, temperature as well as the type and the loading of the B-site cations. Oxygen vacancy formation in Co, Fe, and Mn perovskite-type materials has been studied and the ease of forming oxygen vacancies has been found to increase in the following order: Mn < Fe < Co [12–14]. To take advantage of the stability of Fe and conductivity of Co, oxygen

* Corresponding author at: The Ohio State University, Department of Chemical and Biomolecular Engineering, 140 W 19th Avenue, Columbus, OH 43210, USA. Tel.: +1 614 292 6623; fax: +1 614 292 3769.
E-mail address: Ozkan.1@osu.edu (U.S. Ozkan).

0920-5861/$ – see front matter © 2010 Elsevier B.V. All rights reserved.
doi:10.1016/j.cattod.2010.03.037

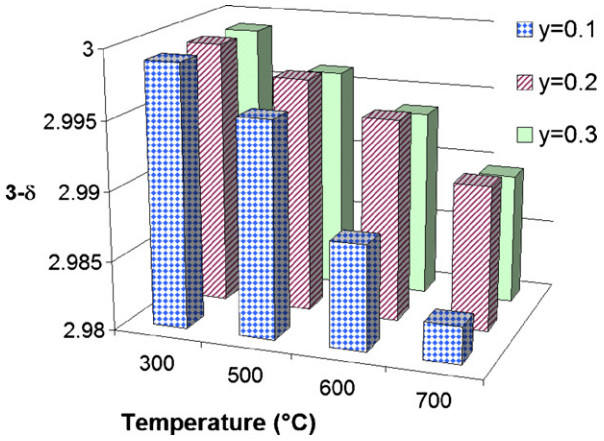

Fig. 1. Temperature programmed oxygen vacancy formation in TGA-DSC for $La_{0.6}Sr_{0.4}Co_yFe_{1-y}O_{3-\delta}$ in air. Adapted from [23].

vacancy formation in solid solutions of Co and Fe has also been studied [15–18].

Compatibility of the electrode with the electrolyte both thermally as well as chemically is another important consideration to be made while selecting cathode materials. The Mn-based materials have shown chemical reactivity problems with yttria-stabilized zirconia (YSZ) electrolyte forming insulating phases such as $La_2Zr_2O_7$, $SrZrO_3$, at the cathode–electrolyte interface [19]. Much of the recent research has also focused on studying the compatibility of the new formulations with the electrolyte materials [20,21].

Our previous work has focused on Fe-based perovskite oxides, especially developing and studying the structure–property relationships of the $La_{0.6}Sr_{0.4}Co_yFe_{1-y}O_{3-\delta}$ materials as a function of the Co content ($y = 0.1$, 0.2 and 0.3) as well as environment and temperature. Several ex situ and in situ methods were used to study the bulk structure of these catalysts. It was found that the unit cell parameters and oxygen content were strong functions of the cobalt content, environment and temperature [23].

In situ XRD was used to determine the unit cell symmetry of these materials as a function of temperature in air. The diffraction patterns for the dominant cubic Miller indices were observed, and the transformation from rhombohedral symmetry to cubic symmetry was observed for the three materials. The transformation was identified by the merging of multiple broad peaks due to the rhombohedral phase to a single sharp peak in the cubic phase. The transition occurred over a range of temperatures, and the temperature at which it was complete was a strong function of the cobalt content. It was seen that, while for the lower cobalt content, the transition required temperatures as high as 800 °C, with increase in Co content, this temperature decreased [23].

Thermo-gravimetric analysis was also used to calculate the oxygen content under different conditions. The oxygen stoichiometry of the sample in air as a function of temperature was determined by TGA and the results are summarized in Fig. 1. It was found that the oxygen vacancies formed more readily and easily for the sample with low Co content. Moreover, the sample with the intermediate Co content had the most difficulty to form oxygen vacancies. With further analysis through Mössbauer spectroscopy, this trend was attributed to an electronic state transition [24].

The surface properties of the $La_{0.6}Sr_{0.4}Co_yFe_{1-y}O_{3-\delta}$ were explored in our prior work and activity for methanol oxidation was studied [25]. The nature of surface sites was explored and quantified using methanol as a probe molecule. The catalysts showed reasonable activity for the methanol oxidation reaction. At lower temperatures and methanol conversions, complete oxidation to CO_2 and H_2O took place over these samples. Again a non-linear trend was observed, with the intermediate Co content showing maximum activity, and this trend follows the same trend as several properties over these materials including amount of basic sites, reducibility, oxygen vacancy generation in air and oxygen storage capacity [23,24]. The current work further explores the properties of these materials as well as compares it with the current state-of-the art cathode material.

2. Experimental

2.1. Sample preparation

Conventional solid-state synthesis methods were used to prepare the catalysts. For $La_{0.6}Sr_{0.4}Co_yFe_{1-y}O_{3-\delta}$ samples, the metal oxide and carbonate precursors were Co_3O_4 (Aldrich), La_2O_3 (Fisher), Fe_2O_3 (J.T. Baker), and $SrCO_3$ (Alfa Aesar). For the $La_{0.6}Sr_{0.4}MnO_3$ catalyst, $MnCO_3$ (Alfa Aesar) was the manganese precursor used. The precursors were first heat treated in air at 550 °C with a 3 h isothermal hold to clean the surface and remove any adsorbed species and to maintain the proper oxidation state. The precursors were then added in stoichiometric proportions (10 g total) to a ceramic milling jar (half pint from U.S. Stoneware) with 1.6–2.5 mm diameter zirconia grinding beads (20 g) and distilled water. The mixture was then ball-milled for 24 h at 120 revolutions per minute using a long roll jar mill. After this, the beads were sieved out and the mixture was allowed to dry on a hotplate and then crushed to powder with a mortar and pestle. The powder was then heated to 1000 °C for 48 h to allow for the high-temperature solid-state reaction to take place, leading to the perovskite structure. The resulting material was again crushed with a mortar and pestle for uniform particle size (between 100 and 150 mesh) distribution.

2.2. X-ray diffraction

Powder diffraction patterns were obtained with a Bruker D8 Advance diffractometer. A Cu $K_{\alpha 1}$ radiation source was used. For room temperature measurements, the sample was loaded on polyethylene holders, and the diffraction patterns were obtained while rotating the sample. The current and the voltage were 50 mA and 40 kV, respectively. The data was collected for 2-θ values from 20° to 90° at a step size of 0.0144° and a dwell time of 1 s.

For in situ measurements, a HTK 1200 sample holder with graphite windows was used, which controls the temperature and atmosphere. Samples were supported on an alumina holder with a 0.5 mm deep reservoir. A heating rate of 10 °C/min and a 20 min hold time (5 min for solid-state reaction) before scanning at each temperature were also employed. The flow rate of air was 10 mL/min.

For the compatibility studies, equal portions of the catalyst and yttria-stabilized (8%) zirconia (YSZ) (Aldrich) were physically mixed and heated to 1400 °C and held at that temperature for 4 h and then cooled. Room temperature XRD patterns were obtained for the resulting mixture. For the in situ monitoring, the $La_{0.6}Sr_{0.4}Co_{0.2}Fe_{0.8}O_{3-\delta}$ and YSZ were mixed and loaded into the alumina holder and a flow rate of 10 mL/min of air and heating rate of 10 °C/min were used.

2.3. Thermo-gravimetric analysis

The oxygen vacancy formation in air was studied using a Setaram TG-DSC111. Flow balancing was done in air at 350 °C. The sample (~85 mg) was loaded into Pt sample cups. After waiting at room temperature for the mass to stabilize, a flow of 15 mL/min of air was started. The sample was then heated to 750 °C at 5 °C/min and was held at that temperature for 30 min before being cooled at the same rate. The temperature program was then repeated and

the mass change from the second program was used to calculate the oxygen vacancy formation. This is done to eliminate effects of surface impurities during the first program.

2.4. NEXAFS analysis

NEXAFS analyses were performed at the U1A beamline of the National Synchrotron Light Source (NSLS) at Brookhaven National Laboratory. The catalyst powder was pressed into a sample holder cup 1 cm in diameter and 0.1 cm in depth. The NEXAFS spectra were recorded at the oxygen K-edge (520–600 eV). The partial electron yields, sensitive mainly to the top few atomic layers [22], were measured as a function of the incident energy with an energy resolution of 0.8 eV at the O K-edge.

2.5. Oxygen temperature programmed desorption

The oxygen temperature programmed desorption (TPD) experiments were conducted on a Thermo-Finnigan Trace Ultra differential scanning quadrupole (DSQ) gas chromatograph/mass spectrometer (GC/MS). The samples were loaded in a quartz U-tube reactor, with plugs of silica glass wool on both ends. The samples (100 mg) were pretreated in 30 mL/min flow of oxygen (20%O_2/He) at 850 °C (10 °C/min) with an isothermal hold for 20 min. The samples were also cooled under the same flow. Once near room temperature (less than 75 °C), the flow was switched to He at 30 mL/min and the lines were purged for 1 h. The sample was then heated to 900 °C at 10 °C/min and held for 20 min. Data from the GC/MS was obtained using selected ion mode (4, 12, 16, 18, 28, 32, and 44 monitored) and a 3 eV detector gain.

2.6. Reaction studies

The catalytic tests were performed on an equal surface area (0.46 m^2) basis using a quartz fixed-bed flow reactor. The catalysts were pretreated in situ under 10%O_2/N_2 (50 cm^3 STP/min) 850 °C for 20 min and cooled under the same flow before reaction. The feed percentages used were $CH_4/O_2/N_2/He = 5/5/40/50$ (feed flow rate 50 cm^3 STP/min). Nitrogen was used as the internal standard to quantify volumetric flow rate. The effluent from the reactor was analyzed using a Shimadzu 2014 Gas Chromatograph which is equipped with a flame ionization detector (FID), pulse discharge helium ionization detector (PDHID) and flame photometric detector (FPD). Separations were performed using He as the carrier gases using two columns: Supelco Q Plot (30 m × 0.53 mm, fused silica capillary column) and Carboxen™ 1010 Plot (30 m × 0.53 mm, fused silica capillary column). Reaction data was acquired after waiting at each temperature for steady state to be reached. Conversions and yields are defined as follows:

$$\%\ CH_4\text{conversion} = \left(\frac{\text{moles of } CH_4 \text{ converted}}{\text{moles of } CH_4 \text{ in feed}}\right) 100$$

$$\%\ O_2 \text{ conversion} = \left(\frac{\text{moles of } O_2 \text{ converted}}{\text{moles of } O_2 \text{ in feed}}\right) 100$$

$$\%\, CO_2 \text{ yield} = \left(\frac{\text{moles of } CO_2 \text{ formed}}{\text{moles of } CH_4 \text{ in feed}}\right) 100$$

3. Results and discussion

3.1. Bulk Characterization using NEXAFS

The O K-edge features for the $La_{0.6}Sr_{0.4}Co_yFe_{1-y}O_{3-\delta}$ samples are shown in Fig. 2. As described in previous reviews [26,27], the O K-edge features are sensitive to the bonding environment and surface concentrations of metal oxides. The peak positions of O K-edge features are similar on all three samples, indicating similar types of oxygen species are present on all samples. However, the intensities and edge jump of the O K-edge features are different, consistent with the different surface oxygen concentrations detected from XPS as well as bulk reducibility observed in TPR [23,25]. In addition it can be seen that, over the sample with 20% Co on the B-site ($y = 0.2$), an additional pretreatment of quenching the catalyst in a nitrogen environment causes a change in the oxygen content and this is directly related to the change in oxidation state-of-the B-site atom [23].

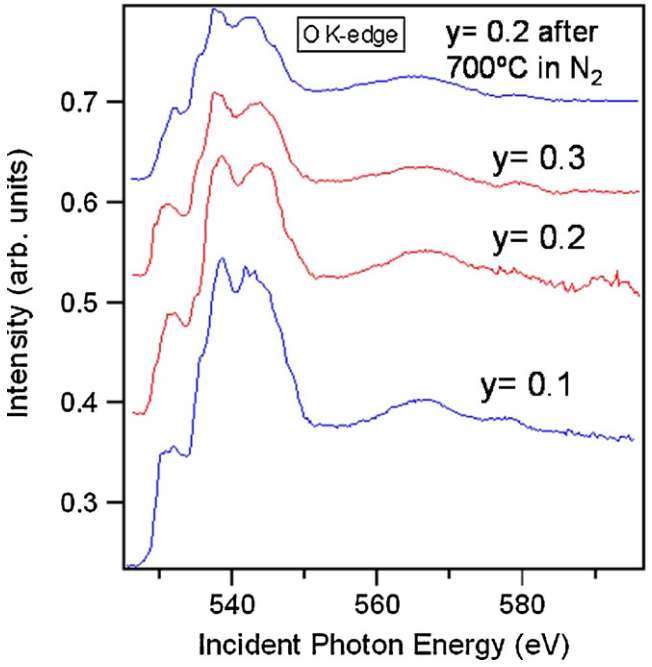

Fig. 2. O K-edge NEXAFS results for $La_{1-x}Sr_xCo_yFe_{1-y}O_{3-\delta}$.

3.2. Oxygen evolution studies—comparison with LSM

The oxygen storage and activation capacity of $La_{0.6}Sr_{0.4}Co_{0.2}Fe_{0.8}O_{3-\delta}$, which showed optimum properties in our previous characterization work, were studied using oxygen temperature

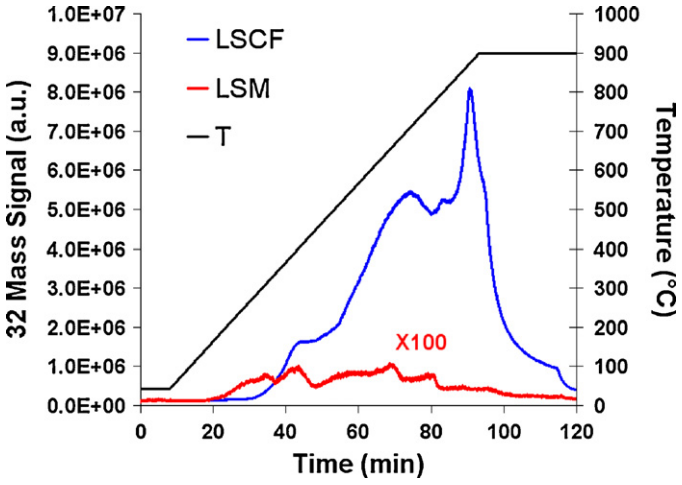

Fig. 3. Temperature programmed oxygen evolution of $La_{0.6}Sr_{0.4}Co_{0.2}Fe_{0.8}O_{3-\delta}$ (LSCF) and $La_{0.6}Sr_{0.4}MnO_3$ (LSM).

programmed desorption (TPD) and the results are compared to that of $La_{0.6}Sr_{0.4}MnO_3$. The nature of oxygen elution from the perovskite materials is well characterized in the literature. Two distinct oxygen peaks are usually observed during TPD: a low temperature evolution called the α desorption and a high-temperature evolution termed β desorption [28]. The α-oxygen is related to reduction of tetravalent cationic species while the β-oxygen comes from the partial reduction of trivalent species and is correlated to the oxygen mobility in the sample. The TPD results for the $La_{0.6}Sr_{0.4}Co_{0.2}Fe_{0.8}O_{3-\delta}$ (LSCF) and $La_{0.6}Sr_{0.4}MnO_3$ (LSM) catalyst is shown in Fig. 3. There is a significantly greater oxygen evolution from the LSCF materials reiterating the increased oxygen mobility and oxygen vacancy formation in these materials.

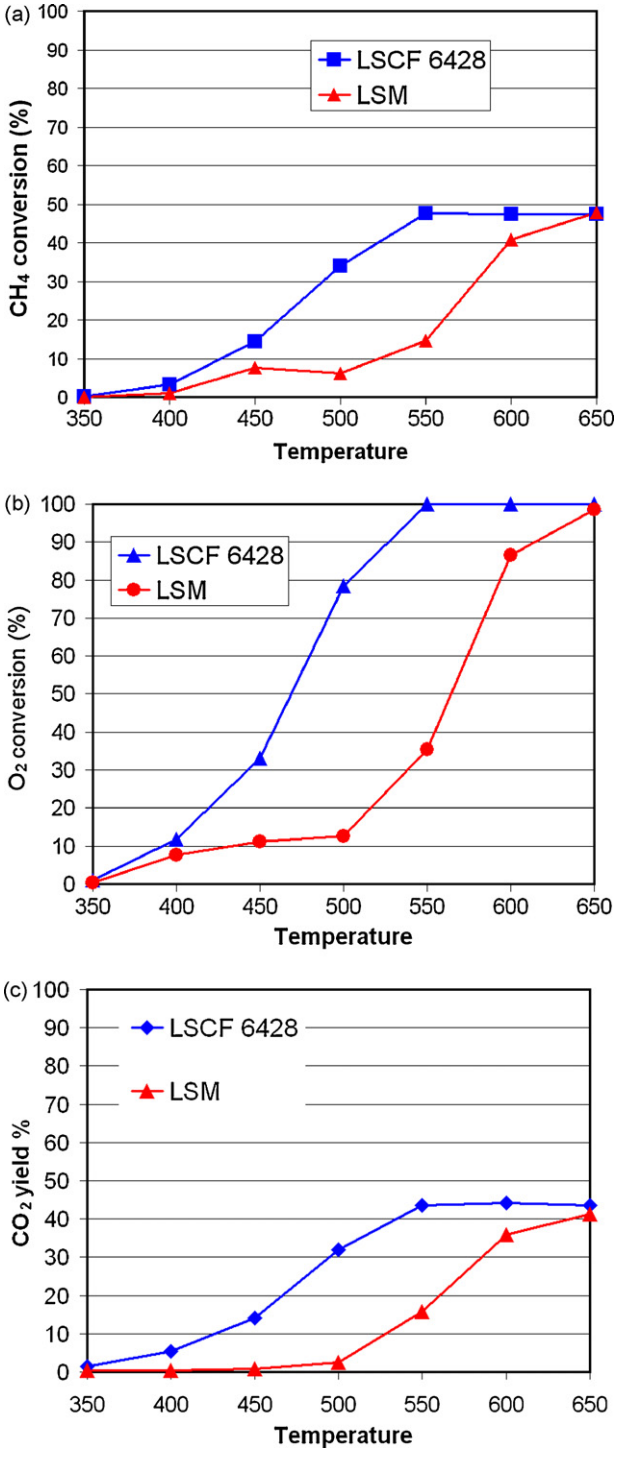

Fig. 4. Steady-state methane oxidation activity of $La_{0.6}Sr_{0.4}Co_{0.2}Fe_{0.8}O_{3-\delta}$ (LSCF 6428) and $La_{0.6}Sr_{0.4}MnO_3$ (LSM): (a) methane conversion (b) oxygen conversion and (c) CO_2 yield.

3.3. Activity for methane oxidation—comparison with LSM

The methane oxidation activity of $La_{0.6}Sr_{0.4}Co_{0.2}Fe_{0.8}O_{3-\delta}$ and $La_{0.6}Sr_{0.4}MnO_3$ was tested and the results are shown in Fig. 4a–c. CO_2 and H_2O were the primary products, and similar to what was observed in the methanol oxidation reaction, completely oxidized products were favored. The activity was comparable to those reported in the literature for these types of materials [2]. The oxygen content in the feed was sub-stoichiometric for the complete oxidation, however, CO_2 was the primary product and no CO was detected. When similar experiments were performed with an on-line mass spectrometer, it was confirmed that CO_2 and H_2O were the only products. In Fig. 4a, it can be seen that over the LSCF catalyst, complete conversion of oxygen was reached by 550 °C. Methane conversions of about 50% were obtained. For the LSM catalyst it can be seen that the activity trails that of the LSCF at lower temperatures. Above 600 °C, the activities are similar and complete conversion of oxygen takes place over both catalysts. The formation of oxygen vacancies in the LSCF materials is probably responsible for higher oxygen conversions due to increased oxygen mobility. During heterogeneously catalyzed reactions, the mechanism of oxidation can be intrafacial (involves mobile lattice oxygen) rather than suprafacial (involves adsorbed oxygen). At temperatures high enough for the bulk oxygen to become mobile, methane oxidation becomes an intrafacial reaction [2]. Thus in the LSCF materials, there is greater bulk-oxygen mobility at lower temperatures, causing almost twofold higher oxygen conversions over these materials at lower temperatures. This property has also led to studies testing the LSCF materials as SOFC anodes [29].

3.4. Chemical compatibility of LSCF with YSZ—comparison with LSM

Chemical compatibility with the electrolyte material was tested using XRD to study the formation of reactive phases like $La_2Zr_2O_7$ and $SrZrO_3$. The electrical conductivity of $La_2Zr_2O_7$ is over 100 times lower than that of YSZ [19]. Mixtures of $La_{0.6}Sr_{0.4}Co_{0.2}Fe_{0.8}O_{3-\delta}$ (LSCF) and YSZ as well as $La_{0.6}Sr_{0.4}MnO_3$ (LSM) with YSZ were heated to 1400 °C and then cooled following which XRD patterns were obtained over both the mixtures. The diffraction patterns are shown in Fig. 5. It can be seen that in both

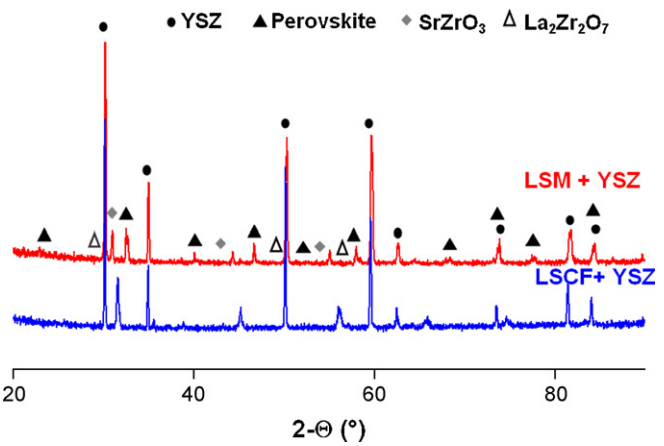

Fig. 5. XRD patterns for mixture of $La_{0.6}Sr_{0.4}Co_{0.2}Fe_{0.8}O_{3-\delta}$ and YSZ (LSCF + YSZ) and $La_{0.6}Sr_{0.4}MnO_3$ and YSZ (LSM + YSZ).

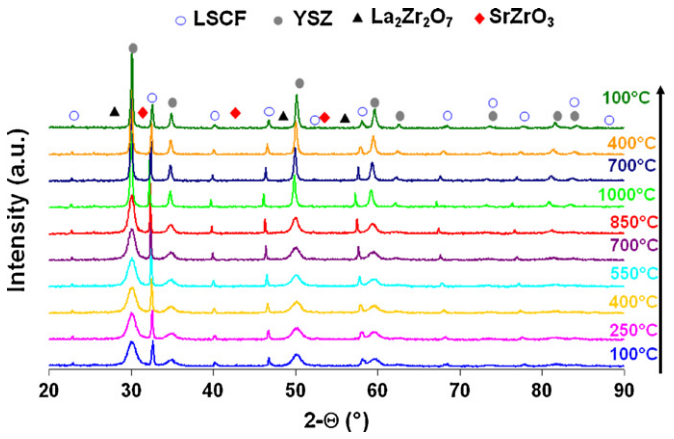

Fig. 6. In situ XRD patterns for mixture of $La_{0.6}Sr_{0.4}Co_{0.2}Fe_{0.8}O_{3-\delta}$ and YSZ.

cases the perovskite phase and the yttria-stabilized zirconia phase were the predominant phases present. In the LSM sample however traces of impurity phases can be detected. The compatibility of the LSCF catalyst was studied in further detail and in situ XRD patterns were obtained for a mixture of $La_{0.6}Sr_{0.4}Co_{0.2}Fe_{0.8}O_{3-\delta}$ and YSZ as a function of temperature; heating and cooling done under air. The diffraction patterns are shown in Fig. 6. No impurity phases were detected, and only the perovskite and YSZ phases were observed. This is in agreement with findings in the literature where it has been shown that Fe doping provides structural stability in Co-based materials [30].

4. Conclusions

The bulk and surface properties of $La_{0.6}Sr_{0.4}Co_yFe_{1-y}O_{3-\delta}$ materials as a function of the Co content ($y = 0.1$, 0.2 and 0.3) were studied. Oxygen storage capacity and oxidation activity of the catalyst with the intermediate Co content were investigated in detail and compared to that of $La_{0.6}Sr_{0.4}MnO_3$. It is found that these materials have an order of magnitude higher oxygen storage capacity, and greater oxygen activation as compared to LSM. The increased oxygen vacancy generation and oxygen mobility in these materials can be responsible for these results. The materials also demonstrated good chemical compatibility with the electrolyte material making them good candidates for intermediate-temperature solid oxide fuel cell cathodes.

Acknowledgments

The financial support provided for this work by the Ohio Coal Development Office and the Ohio Department of Development through a Wright Center of Innovation is gratefully acknowledged. Use of the National Synchrotron Light Source, Brookhaven National Laboratory, for the NEXAFS experiments was supported by the U.S. Department of Energy (DOE/BES Grant No. DE-FG02-05ER15688).

References

[1] L.G. Tejuca, J.L.G. Fierro, J.M. Tascon, Structure and reactivity of perovskite-type oxides, Advances in Catalysis 36 (1989) 237.
[2] M.A. Pena, J.L.G. Fierro, Chemical structures and performance of perovskite oxides, Chemical Reviews 101 (2001) 1981.
[3] L.G. Tejuca, J.L.G. Fierro (Eds.), Properties and Applications of Perovskite-type Oxides, Marcel Dekker, Inc., New York, 1993.
[4] H.J.M. Bouwmeester, H. Kruidhof, A.J. Burggraaf, Importance of the surface exchange kinetics as rate limiting step in oxygen permeation through mixed-conducting oxides, Solid State Ionics 72 (1994) 185.
[5] J.F. Vente, et al., Properties and performance of $Ba_xSr_{1-x}Co_{0.8}Fe_{0.2}O_{3-\delta}$ materials for oxygen transport membranes, Journal of the Electrochemistry Society 10 (2006) 581.
[6] R.M. Ormerod, Solid oxide fuel cells, Chemical Society Review 32 (2003) 17.
[7] S.B. Adler, Factors governing oxygen reduction in solid oxide fuel cell cathodes, Chemical Reviews 104 (2004) 4791.
[8] B.C.H. Steele, Behaviour of porous cathodes in high temperature fuel cells, Solid State Ionics 94 (1997) 239.
[9] S.B. Adler, Mechanism and kinetics of oxygen reduction on porous $La_{1-x}Sr_xCo_{3-\delta}$ electrodes, Solid State Ionics 111 (1998) 125.
[10] S.B. Adler, Limitations of charge-transfer models for mixed-conducting oxygen electrodes, Solid State Ionics 135 (2000) 603.
[11] S.B. Adler, J.A. Lane, B.C.H. Steele, Electrode kinetics of porous mixed-conducting oxygen electrodes, Journal of the Electrochemistry Society 143 (11) (1996) 3554.
[12] J. Mizusaki, M. Yoshihiro, S. Yamauchi, K. Fueki, Nonstoichiometry and defect structure of the perovskite-type oxides $La_{1-x}Sr_xFeO_{3-\delta}$, Journal of Solid State Chemistry 58 (1985) 257.
[13] J. Mizusaki, Y. Mima, S. Yamauchi, K. Fueki, H. Tagawa, Nonstoichiometry of the perovskite-type oxides $La_{1-x}Sr_xCoO_{3-\delta}$, Journal of Solid State Chemistry 80 (1989) 102.
[14] J. Mizusaki, N. Moir, H. Takai, Y. Yonemura, H. Minamiue, H. Tagawa, M. Dokiya, H. Inaba, K. Naraya, T. Sasamoto, T. Hashimoto, Oxygen nonstoichiometry and defect equilibrium in the perovskite-type oxides $La_{1-x}Sr_xMnO_{3+\delta}$, Solid State Ionics 129 (2000) 163.
[15] J.W. Stevenson, T.R. Armstrong, R.D. Carneim, L.R. Pederson, W.J. Weber, Electrochemical properties of mixed conducting perovskites $La_{1-x}M_xCo_{1-y}Fe_yO_{3-\delta}$ (M = Sr, Ba, Ca), Journal of the Electrochemistry Society 143 (9) (1996) 2722.
[16] L.W. Tai, M.M. Nasrallah, H.U. Anderson, D.M. Sparlin, S.R. Sehlin, Structure and electrical properties of $La_{1-x}Sr_xCo_{1-y}Fe_yO_3$. Part 1. The system $La_{0.8}Sr_{0.2}Co_{1-y}Fe_yO_3$, Solid State Ionics 76 (1995) 259.
[17] L.W. Tai, M.M. Nasrallah, H.U. Anderson, D.M. Sparlin, S.R. Sehlin, Structure and electrical properties of $La_{1-x}Sr_xCo_{1-y}Fe_yO_3$. Part 2. The system $La_{1-x}Sr_xCo_{0.2}Fe_{0.8}O_3$, Solid State Ionics 76 (1995) 273.
[18] M.H.R. Lankhorst, J.E. ten Elshof, Thermodynamic quantities and defect structure of $La_{0.6}Sr_{0.4}Co_{1-y}Fe_yO_{3-\delta}$ ($y = 0$–0.6) from high-temperature coulometric titration experiments, Journal of Solid State Chemistry 130 (1997) 302.
[19] R.M. Ormerod, Solid oxide fuel cells, Chemical Society Review (2003) 32.
[20] Zaj, et al., Thermochemical compatibility between selected (La,Sr)(Co,Fe,Ni)O_3 cathodes and rare earth doped ceria electrolytes, Journal of Power Sources 173 (2) (2007) 675–680.
[21] P. Datta, P. Majewski, F. Aldinger, $LaGaO_3$-based cermet for solid oxide fuel cell cathodes, Journal of the European Ceramic Society 29 (8) (2009) 1469–1476.
[22] J.G. Chen, et al., A fluorescence-yield near-edge spectroscopy (FYNES) investigation of the reaction kinetics of NiO/Ni(1 0 0) with hydrogen, Surface Science 279 (1992) 13–22.
[23] J.N. Kuhn, U.S. Ozkan, Effect of Co content upon the bulk structure of Sr- and Co-doped $LaFeO_3$, Catalysis Letters 121 (3–4) (2008) 179–188.
[24] J.N. Kuhn, et al., Oxygen exchange kinetics over Sr- and Co-doped $LaFeO_3$, Journal of Physical Chemistry C 112 (32) (2008) 12468–12476.
[25] J.N. Kuhn, U.S. Ozkan, Surface properties of Sr- and Co-doped $LaFeO_3$, Journal of Catalysis 253 (1) (2008) 200–211.
[26] J.G. Chen, B. Fruhberger, M.L. Colaianni, NEXAFS characterization of compositions and reactivities of transition metal oxides, Journal of Vacuum Science and Technology A14 (1996) 1668–1673.
[27] J.G. Chen, NEXAFS investigations of transition metal oxides, nitrides, carbides, sulfides and other interstitial compounds, Surface Science Reports 30 (1997) 1–152.
[28] T. Seiyama, N. Yamazoe, K. Eguchi, Characterization and activity of some mixed metal oxide catalysts, Industrial & Engineering Chemistry Product Research and Development 24 (1985) 19.
[29] S. Tao, J.T.S. Irvine, Discovery and characterization of novel oxide anodes for solid oxide fuel cells, The Chemical Record 4 (2004) 83–95.
[30] N.A. Merino, et al., Synthesis, characterisation, catalytic activity and structural stability of $LaCo_{1-y}Fe_yO_{3\pm\lambda}$ perovskite catalysts for combustion of ethanol and propane, Journal of Catalysis 240 (2006) 245.